

# Mechanism-Independent Optimization of Combinatorial Nanodiamond and Unmodified Drug Delivery Using a Phenotypically Driven Platform Technology

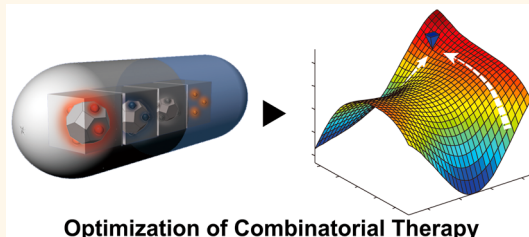
Hann Wang,<sup>†,‡,§,||,⊥,▲</sup> Dong-Keun Lee,<sup>†,‡,§,||,⊥,▲</sup> Kai-Yu Chen,<sup>†,‡,§,||,⊥</sup> Jing-Yao Chen,<sup>#</sup> Kangyi Zhang,<sup>†,‡,§,||,⊥</sup> Aleidy Silva,<sup>¶</sup> Chih-Ming Ho,<sup>\*,¶,||</sup> and Dean Ho<sup>\*,†,‡,§,||,⊥</sup>

<sup>†</sup>Department of Bioengineering, Henry Samueli School of Engineering and Applied Science, <sup>‡</sup>Division of Oral Biology and Medicine, School of Dentistry,

<sup>§</sup>The Jane and Jerry Weintraub Center for Reconstructive Biotechnology, <sup>||</sup>California NanoSystems Institute, <sup>⊥</sup>Jonsson Comprehensive Cancer Center,

<sup>#</sup>Department of Chemical and Biomolecular Engineering, and <sup>\*</sup>Department of Mechanical and Aerospace Engineering, University of California, Los Angeles, California 90095, United States. <sup>▲</sup>H.W. and D.-K.L. contributed equally to this work.

**ABSTRACT** Combination chemotherapy can mediate drug synergy to improve treatment efficacy against a broad spectrum of cancers. However, conventional multidrug regimens are often additively determined, which have long been believed to enable good cancer-killing efficiency but are insufficient to address the nonlinearity in dosing. Despite improved clinical outcomes by combination treatment, multi-objective combination optimization, which takes into account tumor heterogeneity and balance of efficacy and toxicity, remains challenging given the sheer magnitude of the combinatorial dosing space. To enhance the properties of the therapeutic agents, the field of nanomedicine has realized novel drug delivery platforms that can enhance therapeutic efficacy and safety. However, optimal combination design that incorporates nanomedicine agents still faces the same hurdles as unmodified drug administration. The work reported here applied a powerful phenotypically driven platform, termed feedback system control (FSC), that systematically and rapidly converges upon a combination consisting of three nanodiamond-modified drugs and one unmodified drug that is simultaneously optimized for efficacy against multiple breast cancer cell lines and safety against multiple control cell lines. Specifically, the therapeutic window achieved from an optimally efficacious and safe nanomedicine combination was markedly higher compared to that of an optimized unmodified drug combination and nanodiamond monotherapy or unmodified drug administration. The phenotypically driven foundation of FSC implementation does not require any cellular signaling pathway data and innately accounts for population heterogeneity and nonlinear biological processes. Therefore, FSC is a broadly applicable platform for both nanotechnology-modified and unmodified therapeutic optimizations that represent a promising path toward phenotypic personalized medicine.



**KEYWORDS:** nanomedicine · nanodiamond · optimization · drug delivery · breast cancer · biocompatibility

The primary focus of modern cancer drug discovery has largely relied on target and combination-based therapy.<sup>1–3</sup> Despite improvements in treatment outcomes through angiogenic inhibition, antiproliferation, and other targets, issues related to drug resistance, patient toxicity, and suboptimal efficacy persist.<sup>4</sup> Drug resistance is a key challenge that inevitably limits the efficacy of targeted therapy and arises from the innate characteristics of the network of signaling pathways that behaves as a complex system.

A number of biology system studies have shown that cellular pathways form complex networks and that their collective dynamics drive phenotypic outcomes.<sup>5–10</sup> Importantly, network dynamics cannot simply be explained by behavior of an individual component, and as such, therapeutically addressing several elements of a diseased network is important but difficult to optimize at present. Therefore, multi-drug-resistant cancer is one resulting example of a complex system characterized by system robustness, redundant pathways,

\* Address correspondence to  
dean.ho@ucla.edu,  
chihming@seas.ucla.edu.

Received for review January 28, 2015  
and accepted February 17, 2015.

Published online February 17, 2015  
10.1021/acsnano.5b00638

© 2015 American Chemical Society

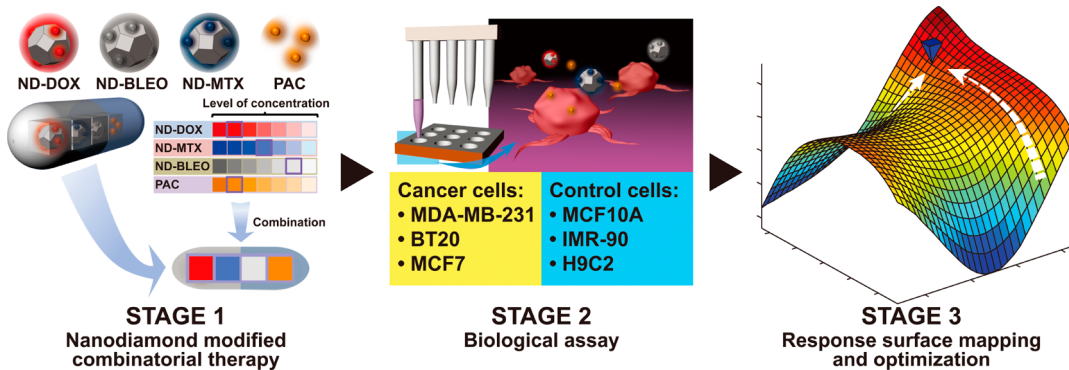


**Figure 1.** Framework of feedback system control. Stage 1: Drug selection/design—doxorubicin (DOX), mitoxantrone (MTX), and bleomycin (BLEO) were loaded onto nanodiamonds (NDs) by physisorption, forming stable and uniform colloidal solutions, and combinations were designed. Latin hypercube sampling was applied on ND-DOX, ND-BLEO, ND-MTX, and PAC to generate 57 combinations of diverse dosing regimens. Stage 2: The 57 combinations were applied to three types of cancer and three types of control cells by customized liquid handling robotic procedures. The viability measurements of three cancer cell lines and three control cell lines were fed into the informatics system. Stage 3: The informatics system generated cellular response surfaces by regression analysis with the customized statistic model on the 57 combinations, which were triplicated and generated in total 171 data points for each cell line. Global combinatorial optimization was carried out by differential evolution on the surface of the therapeutic window. The predicted optimum and randomized combinations were then experimentally verified to ensure mapping accuracy, and the verified global optimum was obtained for further investigation.

cross-talk, antitarget, counter target activity, as well as compensatory and neutralizing actions.<sup>11–16</sup> These complex interactions often render targeted treatment ineffective in the long run.

To address these and other challenges associated with drug-resistant cancer treatment, combination therapy may enhance the systematic modulation of cellular pathways,<sup>17</sup> reducing the likelihood of relapse<sup>18</sup> and showing higher selectivity against cancer cells over healthy cells.<sup>2,17</sup> As such, combination therapy is the clinical standard for multiple cancer treatment regimens.<sup>19–24</sup> However, conventional multidrug regimens are often additively determined where *in vitro* and preclinically efficacious doses are combined and multiplied by a scaling factor for clinical administration. In addition, combinatorial chemotherapy regimens are often added near the maximum tolerated doses, which has been a practice for ensuring cancer-killing efficiency. Despite improvements in clinical outcomes observed following the advent of combination treatment, the multi-end-point optimization of combinatorial therapy is a challenging target given the sheer magnitude of parametric space when considering patient heterogeneity and other factors.

Outside of formulating regimens to deliver multiple drugs to improve treatment outcomes, modifying the drugs themselves to overcome drug resistance and reduce toxicity has been a key focus of the nanomedicine field and resulted in promising findings.<sup>25–45</sup> These approaches resulted in improved intratumoral drug retention, decreased side effects, and improved pharmacokinetic profiles. Therefore, incorporating nanomodified therapies into drug combinations may enable even further enhanced treatment outcomes.

With regards to conventional strategies to improve combination drug dosing, it has long been known that the optimal intervention of drug combinations is dosage-dependent and characterized by therapeutic synergism, additivity, or antagonism. Loewe additivity,<sup>46</sup> Chou–Talalay methods,<sup>47</sup> and Bliss independence method<sup>48</sup> have found utility associated with combination dosing in single enzyme scenarios and were able to examine the nonlinearity of drug–drug interactions. However, a universally applicable platform that operates within the framework of systems-level response and simultaneously addresses the linkage between input stimuli and phenotypic variation across the cellular, tissue, and organism level has not yet been realized. To address this limitation, we have developed the feedback system control (FSC) platform which systematically utilizes three stages to achieve globally optimized combinatorial design. During the past few years, the first generation of FSC (FSC.I) was developed as an iterative feedback search scheme, where 10–20 iterative loops were capable of rapidly identifying optimal combinations from one million or more possible combinations.<sup>49–59</sup> Based on the experimental data obtained via FSC.I, the drug efficacy/dose–response was discovered to be represented by smooth quadratic surfaces.<sup>51</sup> The work reported here, a powerful new platform termed FSC.II, has demonstrated that this smooth surface can be obtained without iterative feedback searches and rapidly interrogated to easily identify the global optimum for efficacy and safety with the most rapid possible convergence rate.

The use of FSC.II to optimize combination nanomedicine drug delivery can be described in three stages (Figure 1). Stage 1 includes the design of the

input stimuli, or drug-dosing regimen. Stage 2 is based on the experimental screening of the phenotypic response of the biological system(s) being interrogated, and stage 3 involves an algorithmically assisted search and convergence toward a global optimum. It should be pointed out that FSC.II is not a modeling platform and is not a predictive approach. Instead, it reconciles experimental findings to construct an optimization profile to pinpoint the global maximum in a deterministic fashion. In stage 1, many ways of selecting drug–dose combinations can be used. Here, we utilized Latin hypercube sampling, which allowed a wide coverage of the concentration domain, to include diversified drug combinations for initial response surface construction.<sup>60</sup> In stage 2, the efficacy and safety of these combinations were assessed in three breast cancer cell lines of varying resistance profiles (MDA-MB-231, MCF7, and BT20) and three control cell lines (breast fibroblast, MCF10A; lung fibroblast, IMR-90; and cardiomyocyte, H9C2) using viability assays to construct therapeutic windows. In stage 3, a response map was then constructed by regression analysis using a tailored dose–response model. The differential evolution optimization protocol<sup>61</sup> subsequently converged upon a global optimum drug combination *within a single experiment*, an improvement over prior FSC.I search modalities which required approximately 10–20 iterations (Figure 1).

While FSC is a broadly applicable platform that can be applied toward both unmodified drugs and feasibly all nanoparticle carriers, nanodiamonds (NDs) were utilized as the drug delivery vehicles for this work and were compared against systematically optimized unmodified drug combinations to demonstrate the broad applicability of FSC.II. NDs represent promising platforms for cancer therapy because they have markedly improved the efficacy and safety of treatment in multiple preclinical studies. Furthermore, they are scalable materials and capable of carrying a broad spectrum of compounds.<sup>62–67</sup> Important studies have previously been carried out to describe the distribution of chemical groups on the surface of the ND particles as well as their unique, facet-dependent electrostatic properties.<sup>68–70</sup> ND surfaces can be harnessed to potently bind a broad range of small-molecule compounds to form ND–drug aggregates that have recently been shown to markedly enhance circulatory half-life as well as efficacy and safety.<sup>41</sup>

The drug candidates for ND-mediated delivery were selected due to multiple factors. For example, the NDs were capable of potently binding DOX, MTX, and BLEO, serving as an important parameter for comparison studies between optimized ND–drug and unmodified drug combinations. In addition, due to the selection of drug-resistant cell lines as testing platforms for FSC.II optimization, the drug compounds utilized served as relevant inputs for this study. Unmodified paclitaxel

was selected due to its role as a cytoskeletal therapeutic to complement the varying DNA-related mechanisms of action mediated by DOX, MTX, and BLEO that could be even further enhanced by ND modification.

Optimal combinations composed of three ND–drug combinations including ND–doxorubicin (ND–DOX), ND–nitoxantrone (ND–MTX), and ND–bleomycin (ND–BLEO) as well as unmodified paclitaxel (PAC) were shown to outperform randomly formulated combinations, combinations of unmodified compounds, as well as both nanodiamond-modified and unmodified single drug regimens. Rather than account for all of the signaling pathway behavior and genotypic properties of the biological system being addressed, the approach reported here rationally reconciled biological phenotypic response to therapeutic perturbation. Using this platform, we did not rely on complex modeling or theoretical assumptions to predict a treatment outcome. Rather, experimental validation of cellular outcomes from drug intervention was directly used to deterministically converge upon a multiparametric, optimum drug combination. Therefore, the FSC.II platform serves as an efficient route toward globally optimal combination drug development.

## RESULTS AND DISCUSSION

**Nanodiamond–Drug Synthesis.** In order to confirm the presence of DOX, MTX, and BLEO on the NDs, Fourier transform infrared spectroscopy (FTIR) spectra were assessed by comparing the peaks of NDs, unmodified drugs, and ND–drugs (Figure 2A). In the spectral region of 1700 to 1800 cm<sup>−1</sup>, all ND–drugs contained broad stretching vibrations of C=O from various carbonyl species formed on the ND surfaces, such as ketone, ester, lactone, and carboxylic acid. The peak at 1632 cm<sup>−1</sup> represented the bending vibration of O–H from adsorbed water on the NDs. In addition, the vibrational spectra observed with each unmodified drug and ND–drug complexes showed similar profiles overall and identical vibrations in specific bands related to key functional groups of each drug molecule. In addition, vibration bands at 780–850, 1560–1590, 1603–1616, and 1620–1650 cm<sup>−1</sup> that were clearly visible from the ND–drug samples were noticeably absent in the ND-only samples. These peaks are indicative of C=C–H out-of-plane bending vibrations, with two peaks representing C=C stretching vibrations and C=O stretching vibrations. Due to the interaction between the NDs with benzene double bonds and other π bonds, the C=O stretching vibration was observed at a wavenumber lower than the usual C=O stretching vibration.

Particle size comparisons between drug-loaded and unmodified NDs were performed by dynamic light scattering analysis. The hydrodynamic diameter of NDs in water was  $46.6 \pm 0.17$  nm (Figure 2B). Following drug adsorption, the hydrodynamic diameters of ND–DOX,

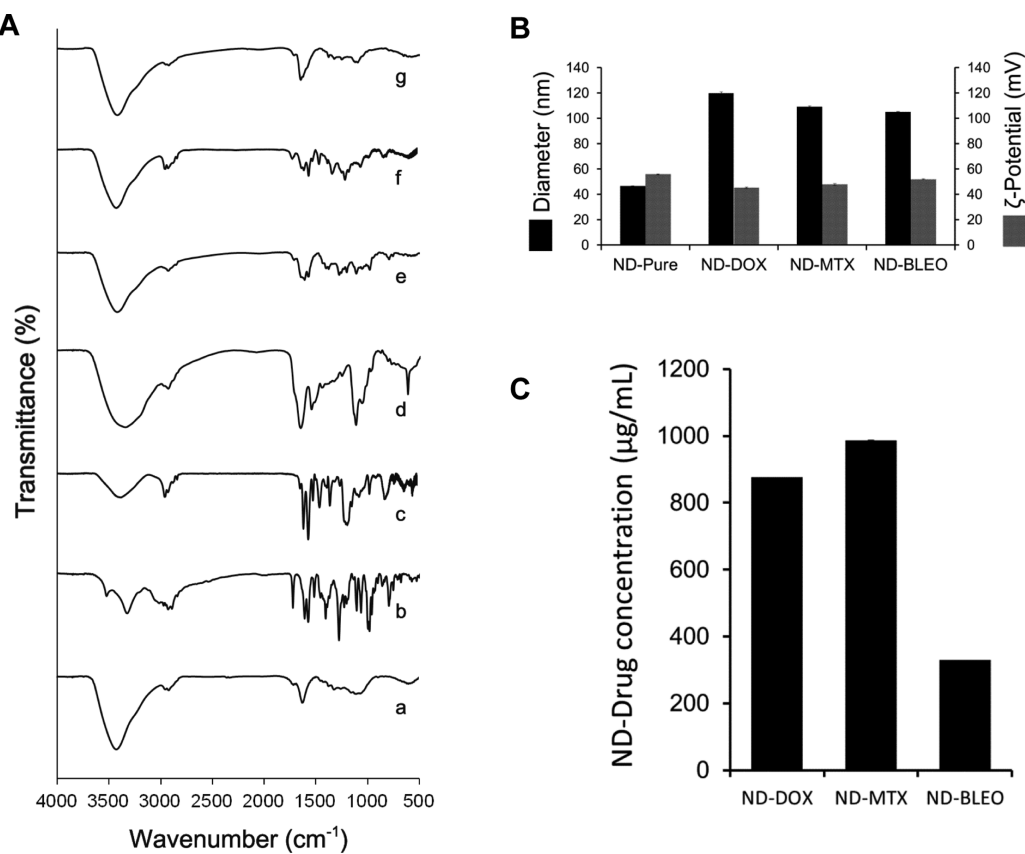


**Figure 2.** Nanodiamond–drug synthesis and characterization. (A) FTIR spectra of (a) nanodiamond (ND), (b) doxorubicin (DOX), (c) mitoxantrone (MTX), (d) bleomycin (BLEO), (e) ND–DOX, (f) ND–MTX, and (g) ND–BLEO. (B) Dynamic light scattering analysis for the ND and ND–drugs. The graph shows that the diameters of ND, ND–DOX, ND–MTX, and ND–BLEO are  $46.6 \pm 0.17$ ,  $120.0 \pm 0.93$ ,  $109.2 \pm 0.58$ , and  $105.1 \pm 0.53$  nm ( $n = 5$ ), and  $\zeta$ -potentials of ND, ND–DOX, ND–MTX, and ND–BLEO are  $55.8 \pm 0.37$ ,  $45.3 \pm 0.51$ ,  $47.8 \pm 0.66$ , and  $52.0 \pm 0.35$  mV ( $n = 3$ ), respectively. (C) Drug concentrations on the NDs in 1 mL of ND–drug solution. Drug concentrations of DOX, MTX, and BLEO in each 1 mL of ND–drug solution are  $876 \pm 2.8$ ,  $987 \pm 1.0$ , and  $329 \pm 1.0$   $\mu\text{g}$ , respectively ( $n = 3$ ).

ND–MTX, and ND–BLEO were increased to  $120.0 \pm 0.93$ ,  $109.2 \pm 0.58$ , and  $105.1 \pm 0.53$  nm, respectively, confirming ND–drug interaction. Additionally,  $\zeta$ -potential measurements were performed (Figure 2B). While the  $\zeta$ -potential of NDs was observed to be  $55.8 \pm 0.37$  mV, the  $\zeta$ -potentials of ND–drug complexes were slightly reduced to  $45.3 \pm 0.51$  (ND–DOX),  $47.8 \pm 0.66$  (ND–MTX), and  $52.0 \pm 0.35$  mV (ND–BLEO). Conclusively, both ND and ND–drugs show a narrow size distribution and similar  $\zeta$ -potentials in each sample, which indicates good homogeneity of particles in media. These are important properties in a scalable and translationally relevant drug delivery system.

To determine the amount of drugs conjugated, UV spectroscopy was studied as described in Materials and Methods (Figure 2C). We measured the absorbance of the supernatants at 550 nm for DOX, 590 nm for MTX, and 290 nm for BLEO and calculated the concentrations of drugs bound to the NDs via a standard curve derived by specific serial concentrations of drugs (Supporting Information Figure S1). The loading efficiencies of ND–DOX, ND–MTX, and ND–BLEO were  $876 \pm 2.8$ ,  $987 \pm 1.0$ , and  $329 \pm 1.0$   $\mu\text{g}$ , respectively.

#### Feedback System Control Optimization of Nanodiamond Combinations.

The drug combination utilized for this study was based on a panel of four drugs, including three that were ND-modified: ND–DOX, ND–BLEO, and ND–MTX, as well as one unmodified drug, PAC. The dose–response curves of the panel of drugs were constructed by conducting a nine-stage 2.5-fold serial dilution on a panel of six cell lines, including three cancer cell lines of varying levels of drug resistance, MDA-MB-231, BT20, and MCF7, and three control cells, MCF10A, H9C2, and IMR-90. The dose–response curves were applied to determine the concentration domain of each drug in each cell, which resided between the maximum applicable concentration and the no response concentration (cell death <5%). For each drug, the final concentration domain was determined so that it covered the concentration domain of all cell lines. The concentration of each drug was discretized for FSC.II into seven dilution stages in log scale to cover the specified range (Table S1). Latin hypercube sampling generated 57 drug combinations that consisted of different four-drug concentrations from the panel of drugs (Table S2).<sup>60</sup> The number of

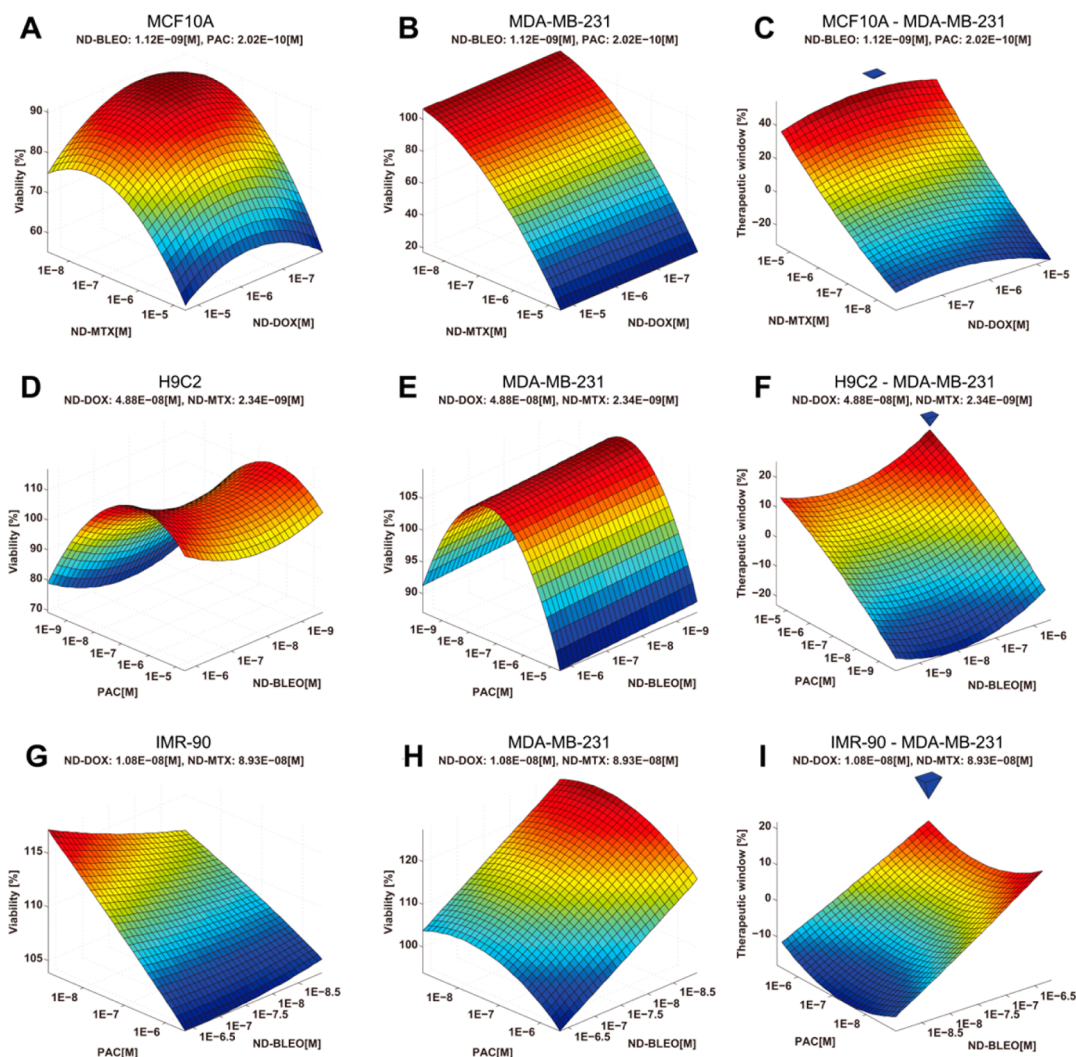


**Figure 3.** Formation of the therapeutic window surface from the cellular response surfaces. (A) Response surface showing the cellular response of the MCF10A (control) cells to varying combinations of ND-DOX, ND-BLEO, ND-MTX, and PAC. The concentrations of ND-BLEO and PAC were fixed at optimal dosage, while the surface was plotted by varying the concentration of ND-MTX and ND-DOX. Two dimensions (concentrations) were fixed in order to project the full five-dimensional surface in three dimension ( $n = 3$ ). (B) Response surface showing MDA-MB-231 (triple-negative breast cancer) cellular response to the ND combinations ( $n = 3$ ). (C) Therapeutic window surface between the MDA-MB-231 (cancer) and MCF10A (control) cells when the four-drug combinations were applied ( $n = 3$ ). The concentration levels were reversed to enable a better viewing angle of the higher therapeutic window surface area. The blue pyramid denotes the experimentally verified optimal therapeutic window,  $51.50 \pm 3.51\%$ , with the bottom tip of the pyramid representing the experimental mean and the height of the pyramid representing the standard error. The dosing of the optimum ND combination was ND-DOX =  $9.88 \times 10^{-7}$  M, ND-BLEO =  $1.12 \times 10^{-9}$  M, ND-MTX =  $2.10 \times 10^{-5}$  M, and PAC =  $2.02 \times 10^{-10}$  M. The FSC predicted that the optimum therapeutic window was located at the same concentration as the pyramid and had a value of 47.01%. A *t* test generated a *p* value of 0.35 (null hypothesis holds true), indicating that the FSC prediction was statistically significant to predict the experimental optimum. (D) Response surface of H9C2 ( $n = 3$ ). (E) Response surface of MDA-MB-231 ( $n = 3$ ). (F) Therapeutic window surface between H9C2 (control) and MDA-MB-231 (cancer) ( $n = 3$ ). The experimental optimal therapeutic window was  $21.46 \pm 4.00\%$  and located at ND-DOX =  $4.88 \times 10^{-8}$  M, ND-BLEO =  $2.00 \times 10^{-6}$  M, ND-MTX =  $2.34 \times 10^{-9}$  M, and PAC =  $2.00 \times 10^{-5}$  M; predicted optimal is 20.71% (*p* = 0.78). (G) Response surface of IMR-90 ( $n = 3$ ). (H) Response surface of MDA-MB-231 ( $n = 3$ ). (I) Therapeutic window surface between IMR-90 (control) and MDA-MB-231 (cancer) ( $n = 3$ ). The experimental optimal therapeutic window was  $15.80 \pm 6.19\%$  and located at ND-DOX =  $1.08 \times 10^{-8}$  M, ND-BLEO =  $4.47 \times 10^{-7}$  M, ND-MTX =  $8.93 \times 10^{-8}$  M, and PAC =  $2.94 \times 10^{-5}$  M; predicted optimal is 9.53% (*p* value = 0.48).

combinations was chosen to be 57 to enable definitive convergence to global optimal for *in vitro* and preclinical experimental validation and ensure that it exceeds the minimum required sample size for multiple regression studies to achieve desired statistical power given the anticipated effect size.<sup>71</sup> The combinations were then added to the cell lines by a customized liquid handling

robotic procedure in a high-throughput format, and the viabilities of the cells were measured by resazurin assay. The five-dimensional cellular response surfaces were constructed with the experimental viability data sampled by Latin hypercube (Figure 3A,B,D,E,G,H).

The response surfaces and therapeutic window surfaces are based on sections of five-dimensional

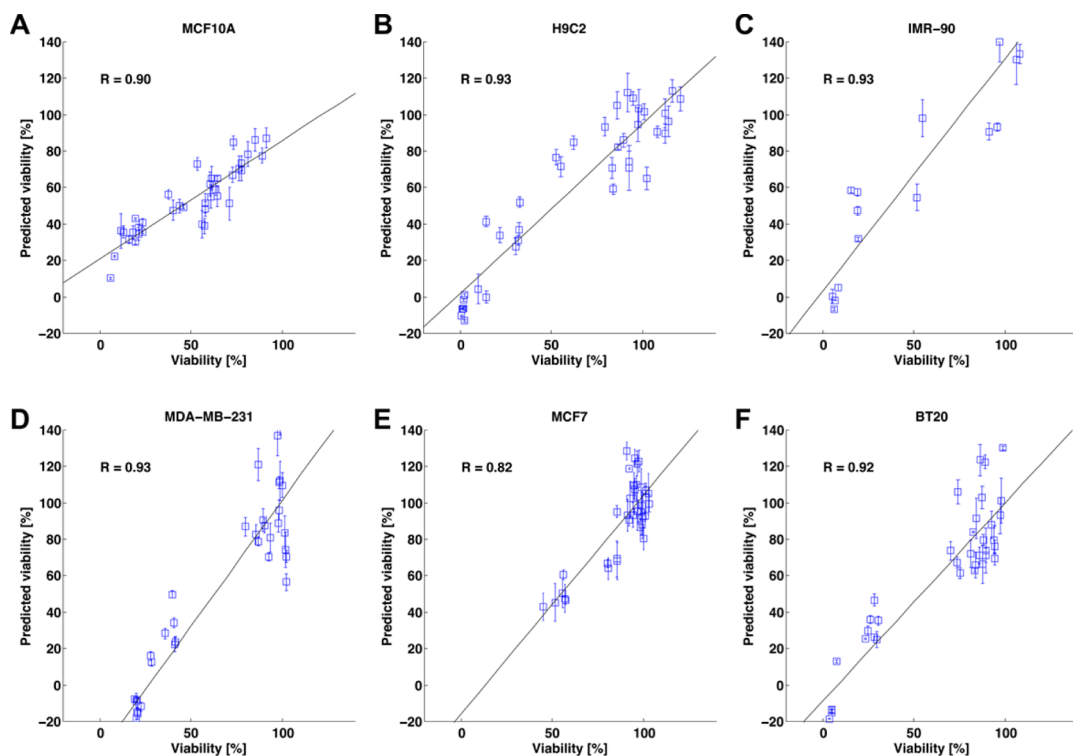


**Figure 4.** Pearson correlation plot for verification experiment *versus* model prediction. Pearson correlation plots of the FSC-predicted viabilities of (A) MCF10A, (B) H9C2, (C) IMR-90, (D) MDA-MB-231, (E) MCF7, and (F) BT20 *versus* experimental values ( $n = 3$ ) of these three control cells and three cancer cells in the verifications, showing high correlation of  $R = 0.90, 0.93, 0.93, 0.93, 0.82$ , and  $0.92$ , respectively, between predicted values and experimental values ( $n = 3$ ).

surfaces (Figure 3A–I), from which two drugs are fixed as an anchor point and the surface is plotted by varying the concentration of the two other drugs. The differential evolution optimization protocol<sup>61</sup> was applied onto the five-dimensional surface of the therapeutic window to locate the global optimal dosage of the cell pair composed of one cancer cell and one healthy cell. We subsequently experimentally verified the efficacy of the identified optimum. The quality of the response surfaces was ensured by including randomized combination samples in the verification experiments. To compare the FSC.II therapeutic window prediction with experimental verification, a *t* test with the hypothesis that the experimental window was derived from normal distribution with the mean as the prediction and unknown variance was conducted. Therefore, the null hypothesis will pass if the prediction and experimental values match. The blue pyramid denotes the experimentally verified optimal therapeutic window for MCF10A and MDA-MB-231 (Figure 3C), which was shown to be  $51.50 \pm 3.51\%$ , with the bottom tip of the pyramid representing the experimental mean and the height of the pyramid representing the standard deviation. The specific drug doses that comprised the optimum ND combination were ND–DOX =  $9.88 \times 10^{-7}$  M, ND–BLEO =  $1.12 \times 10^{-9}$  M, ND–MTX =  $2.10 \times 10^{-5}$  M, and PAC =  $2.02 \times 10^{-10}$  M. Of note, the FSC-prescribed optimum therapeutic window was located at the same concentration as the

experimentally verified dose represented by the pyramid and had a value of 47.01%. The cases of H9C2 *versus* MDA-MB-231 and IMR-90 *versus* MDA-MB-231 are shown in Figure 3F,I, respectively. The experimental optimal therapeutic window was shown to be close to the FSC prediction with high *p* values (0.78 and 0.47, respectively). The FSC predictions were compared with verification results, and a Pearson correlation was determined to assess the accuracy (Figure 4). Importantly, in each experimental condition, it was clear that FSC.II can effectively and accurately predict the result and converge on an experimentally verified optimum.

**Feedback System Control-Optimized Nanodiamond Combinations Outperform Single Drugs.** In order to confirm that the FSC-optimized drug combinations outperform single drug administration, the performance, which was measured by a therapeutic window, of single drugs and the ND combination drug was experimentally determined on a panel of six cell lines, including cancer cell lines, MDA-MB-231, MCF7, and BT20, and three control cells, MCF10A, H9C2, and IMR-90 (Figure 5 and Figure S2). Each individually administered drug, both unmodified and ND-modified, was serially diluted and applied to the panel of six cell lines; the optimal dosages, which generated the highest therapeutic window in each cancer and control pair, were determined by the optimal experimental result. The optimal ND combination for each cancer and control pair was prescribed by FSC and experimentally verified. Given that the dosing

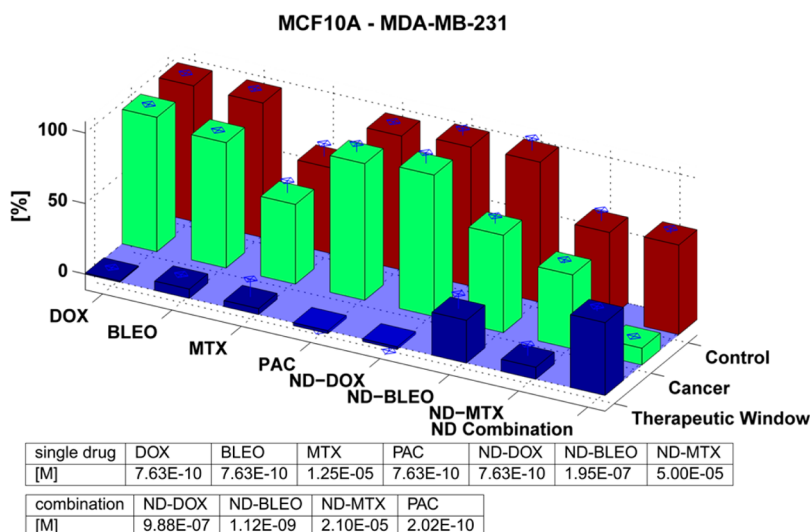


**Figure 5.** Nanodiamond combination performance *versus* nanodiamond single drug administration. Bar graph showing the therapeutic window between the viabilities of the cancer cell, MDA-MB-231, and control cell, MCF10A, from the optimum dosing of each drug or drug combination in the experiment ( $n = 3$ ). The length of the vertical blue line shows the standard error of each condition. The concentration of optimal dosing is provided in the table at the bottom.

of all possible drug combinations encompassed that of the single drug, the therapeutic window of the global optimal combination was expected to outperform all single drugs.

In comparing the FSC-optimized ND combination with optimal single drug administration, it was observed that the ND combination outperforms all of the single drugs as measured by the therapeutic window of MCF10A and MDA-MB-231 (Figure 5). The optimal ND combination-mediated therapeutic window was  $51.50 \pm 3.51\%$ , and the best single-drug-mediated therapeutic window was  $30.22 \pm 10.62\%$  via ND-BLEO. Therefore, the optimal ND combination outperformed the best single drug by 21.28%. Interestingly, the main effector compounds in the optimal ND combination were ND-DOX and ND-MTX, but not ND-BLEO, which was the best performing single drug. In addition, it could clearly be seen that the rational design of a ND-modified drug combination resulted in markedly different drug concentrations from the single drugs (table in Figure 5).

**FSC-Optimized Nanodiamond Combinations Outperform Optimal Unmodified Combination Drugs.** In addition to comparing ND-modified drug performance against single-drug-mediated therapeutic windows, a comparative study between FSC-optimized ND-drug combinations and unmodified drug combinations was performed. The optimal ND-modified and unmodified combinations of DOX, BLEO, MTX, and PAC were determined via FSC.II on a panel of four cell types, including one cancer cell line, MDA-MB-231, and three control cells, MCF10A, H9C2, and IMR-90 (Figure 6). To evaluate whether optimal ND combination outperforms that of unmodified, we tested the null hypothesis that the difference of two therapeutic windows came from normal distribution with zero mean

and unknown variance, using the paired-sample *t* test. In the case of MCF10A *versus* MDA-MB-231, the therapeutic window of the optimal ND combination and unmodified combination was  $51.50 \pm 3.51$  and  $31.10 \pm 2.50\%$ , respectively. Therefore, the optimal ND combination therapeutic window outperformed the optimal unmodified combinations by 20.40% ( $p = 0.0146$ , Figure 6A). In the case of H9C2 *versus* MDA-MB-231, the therapeutic window of the optimal ND combination and unmodified combination was  $21.46 \pm 4.00$  and  $4.94 \pm 5.06\%$ , respectively. Therefore, the optimal ND combination outperformed the optimal unmodified combination by 16.52% ( $p = 0.0012$ , Figure 6B). In the case of IMR-90 *versus* MDA-MB-231, the therapeutic window of the optimal ND combination and unmodified combination was  $15.80 \pm 6.19$  and  $2.20 \pm 3.66\%$ , respectively. In this scenario, the optimal ND combination outperformed the optimal unmodified combination by 13.6% ( $p = 0.0301$ , Figure 6C). Figure 6A–C indicated that the FSC-prescribed ND-drug combinations comprised markedly different drug doses toward the mediating of rationally improved therapeutic windows. Importantly, these values demonstrate that FSC can converge on specific drug ratios that mediate these optimal responses. ND-modified drugs can overcome issues such as drug resistance or improve intratumoral retention, among other benefits which likely serve as foundations for the improved efficacy of ND-modified drug combinations over unmodified combinations.

**FSC-Optimized Nanodiamond Combinations Outperform Randomly Sampled ND-Drug Combinations.** Additive or dose escalation-designed drug combinations are current clinical standards that are virtually precluded from mediating optimal therapeutic efficacy and safety.<sup>19–24</sup> Given the sheer magnitude of the entire therapeutic search, it

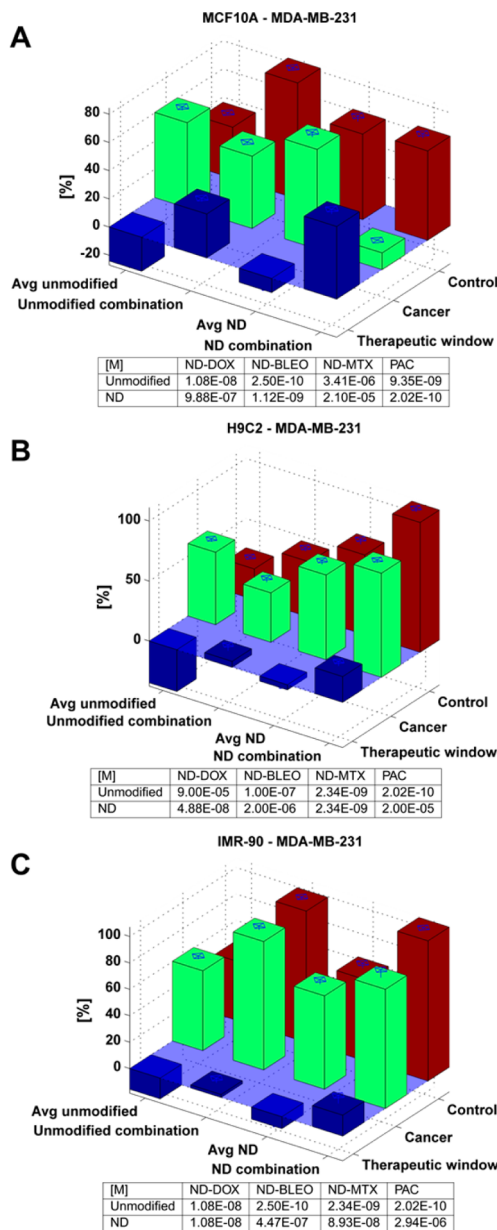


**Figure 6. Nanodiamond combination performance versus unmodified combinations.** (A) Therapeutic window of the optimal ND combination versus optimal unmodified combination for MCF10A (control) and MDA-MB-231 (cancer cell) ( $p = 0.0146$ ,  $n = 3$ ); the average performance of unmodified and ND combination is also listed. Notice that the optimal composition of drug concentration is different for ND and unmodified combinations. (B) Therapeutic window of the optimal ND combination versus optimal unmodified combination in the case of H9C2 (control) and MDA-MB-231 (cancer cell) ( $p = 0.0012$ ,  $n = 3$ ). (C) Therapeutic window of the optimal ND combination versus optimal unmodified combination in the case of IMR-90 (control) and MDA-MB-231 (cancer cell) ( $p = 0.0301$ ,  $n = 3$ ).

is unlikely that a randomized sampling method can accurately locate the global optimum. We compared the performance (therapeutic window) of randomly sampled ND-drug combinations with that of an FSC-optimized ND combination and showed that randomized combinations usually lead to suboptimal results.

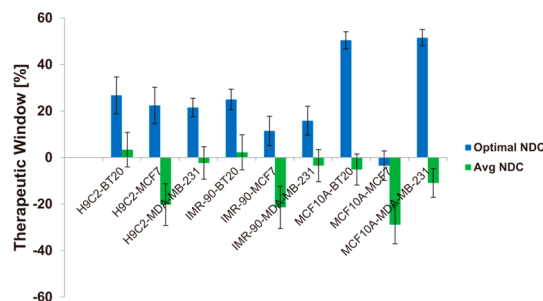


**Figure 7. Nanodiamond optimum combination performance versus nanodiamond randomized combinations.** The therapeutic windows of a panel of cancer and control pairs are shown. Cancer cell lines include MDA-MB-231, MCF7, and BT20 and control cells include MCF10A, H9C2, and IMR-90, forming a total of six possible cancer control pairs ( $n = 3$ ).

Specifically, we took the average experimental therapeutic window of the 57 randomized combinations obtained via Latin hypercube sampling and compared this value with the experimental optimal combination found out by FSC (Figure 7). In the case of H9C2 versus MCF7, the optimal dosage outperformed the average significantly by 42.66% ( $p = 6.39 \times 10^{-4}$ , Table S3). In the most extreme case, MCF10A versus MDA-MB-231, the optimal ND combination outperformed the average combination by 62.43% ( $p = 9.39 \times 10^{-18}$ , Table S3). Furthermore, among the 57 random combinations sampled, we found that only 22.8% of the samples mediated a positive therapeutic window. It should also be noted that the application of random sampling methods such Gaussian distribution or uniform distribution over an FSC-prescribed 57 combination search would have resulted in an even lower percentage of samples exhibiting a positive therapeutic window. Provided that a random sampling method samples the space uniformly, the likelihood of consistently finding a combination with a positive therapeutic window is highly challenging and therefore requires that a systematic and rational platform, such as FSC technique, be utilized to enable convergence toward a global optimum.

**Reconciling Phenotypic Information To Optimize Nanodiamond–Drug Combinations.** In this study, DOX, MTX, and BLEO were selected because they bind potently and rapidly to the NDs. In addition, the ND–drug interaction has been shown to markedly reduce toxicity while the drug is being carried.<sup>41,43,45,72</sup> Specifically, we have previously shown that the ND–drug agents markedly improved drug tolerance when carried, such that treatment toxicity was reduced or eliminated via ND binding. Therefore, the ND served as a scalable delivery agent for rapid nanomodified drug synthesis that simultaneously improved drug safety and tolerance. Unmodified PAC was utilized to demonstrate the modular nature of FSC and its ability to deliver a combination of both nanomodified and unmodified therapeutic agents. While the nanodiamond-modified

drugs used in this study were similar in structure and function, they served as model chemotherapeutic agents, and the ND carrier and FSC platform are capable of being adapted toward virtually any therapeutic compounds for other indications, as well.

The phenotype (e.g., viability) of a diseased biological complex system (cell, animal, and human) under drug treatment can be expressed as a function,  $V(\mathbf{s}, \mathbf{x})$ , of the disease-causing mechanisms,  $\mathbf{s}$ , and the drug concentrations,  $\mathbf{x}$ . According to the Taylor expansion in mathematics,  $V(\mathbf{s}, \mathbf{x})$  can be related to the diseased biological complex system before therapeutic intervention,  $V(\mathbf{s}, \mathbf{0})$ , as

$$V(\mathbf{s}, \mathbf{x}) = V(\mathbf{s}, \mathbf{0}) + \sum_k a_k x_k + \sum_l b_l x_l^2 + \sum_m \sum_n c_{mn} x_m x_n + \text{high order terms}$$

It has been found that the high-order terms are much smaller than the first- and second-order terms.<sup>51,73</sup> We can then write the efficacy of the combinatorial drugs as

$$V(\mathbf{s}, \mathbf{x}) - V(\mathbf{s}, \mathbf{0}) \approx \sum_k a_k x_k + \sum_l b_l x_l^2 + \sum_m \sum_n c_{mn} x_m x_n$$

Due to the complexities of the disease-causing mechanisms in the genome and in protein networks, the explicit functions of  $V(\mathbf{s}, \mathbf{x})$  and  $V(\mathbf{s}, \mathbf{0})$  for the diseases are unknowns. However, the efficacy, that is, the differences of the two equations, can be expressed by a simple quadratic algebraic series. A small number of tests in various dose combinations can determine the coefficients of algebraic series and locate the optimal dose combination from a very large combinatorial drug–dose parameter space. In other words, the FSC technique can bypass the identification of the disease-causing mechanisms and to home in the optimal treatment of achieving the multidimensional desired end point outputs.

The fitted response surfaces of two selected cancer and control cell pairs were superimposed to form a five-dimensional surface of therapeutic window  $h(\mathbf{x})$ , where  $h(\mathbf{x})$  is defined as

$$h(\mathbf{x}) = \text{FSC}_{\text{control}}(\mathbf{x}) - \text{FSC}_{\text{cancer}}(\mathbf{x})$$

where  $\text{FSC}_{\text{control}}(\mathbf{x})$  and  $\text{FSC}_{\text{cancer}}(\mathbf{x})$  are the viability for control cells and cancer cells, respectively. In fact, the most powerful feature of FSC is the ability to be able to superimpose multiple response surfaces to achieve simultaneous multi-objective optimization. We defined  $h$  as the superposition of two cells in this paper for simplicity of interpretation as well as proof of principle.

An important aspect of this study has highlighted the fact that, due to synergistic and antagonistic effects between different drugs, therapeutic efficacy cannot simply be determined by multiple dose–response curves of the single drugs. Instead, the therapeutic window is in fact fully represented by a multidimensional

response surface. The optimal dosage or combination of drugs that can maximize the therapeutic window is located within this multidimensional response surface. For instance, a  $N$  drug combination with  $D$  different concentrations will result in  $DN$  possible combinations. Conventional methods (e.g., high-throughput screening) are a measure-all approach, which is inefficient because the possible number of drug combinations grows exponentially with each increase in the number of drugs that comprise the combination. Furthermore, the measure-all approach cannot be extended to *in vivo* or clinical trials. FSC.II has thus demonstrated a unique advantage in this case, resolving the complete response surface with the smallest possible number of experiments while rapidly homing in the global optimum.

**Multiparametric Optimization of Nanodiamond–Drug Combinations via Feedback System Control.** An important finding following the demonstration that FSC-optimized ND combinations outperform single drug efficacy and safety was that most of the single drugs did not mediate a large therapeutic window. For example, DOX, BLEO, MTX, and ND–MTX exhibited therapeutic windows of less than 10% and thus did not have a major therapeutic effect. Single drug administration still serves as a clinical standard of treatment for several cancers, and it is well-known that innate or acquired drug resistance and a decline in efficacy, as well as toxicity, remain major obstacles to single drug administration.<sup>74–77</sup> To overcome these issues, nanomedicine has been used to overcome resistance and reduce toxicity in preclinical and now clinical studies.<sup>36,78</sup> Since combination therapy is a widely adopted strategy to even further enhance treatment efficacy, these findings confirm the use of combination nanotherapy to improve treatment efficacy over single unmodified drug or nanodrug administration.

Because FSC.II is a platform technology, it can easily be applied to a broad range of other drugs (nanomodified or unmodified) and nanomaterial platforms that have been shown to improve therapeutic outcomes.<sup>38–40,79,80</sup> This is due to the fact that a nanomodified therapeutic serves as an input while the phenotypic response from the biological system represents an output, and FSC.II constructs a response map to specifically pinpoint drug ratios that reach a global maximum where efficacy and safety can be optimized. This study utilized ND-functionalized DOX, MTX, and BLEO as well as unmodified paclitaxel and drug combinations without the NDs as examples of inputs that can be optimally prescribed via FSC.II to demonstrate its applicability to a broad spectrum of therapeutic compounds and nanomaterials to formulate optimal nano and non-nanodrug combinations.

The ability to rationally design and experimentally verify a globally optimized ND-modified drug combination from this portion of the study also highlights the ability for FSC to systematically address the

issue of resistance in cancer. The selected BT20, MCF7, and MDA-MB-231 cancer cell lines each possess varying drug resistance profiles,<sup>81–83</sup> and the ability for the FSC platform to rapidly converge upon an optimum combination that accounts for this resistance thus allows for a dynamic response to the cancer cells' ability to evolve against drug-induced cytotoxicity. Therefore, in a scenario where a drug, either unmodified or ND-modified, is rendered inactive against a particular type of cancer, this drug can be removed from combinatorial design and replaced with a new candidate compound. A subsequent redesigned, globally optimized combination can then be prescribed and verified for rapid implementation. Importantly, it should also be noted that following the *in vitro* selection of FSC-optimized drug combination candidates as shown in this study, downstream preclinical and translational optimization is capable of using additional FSC-inspired drug design platforms that can multiparametrically maximize safety and efficacy.

## CONCLUSIONS

In summary, this work has demonstrated the rapid and multiparametric optimization of both nanoparticle and unmodified drug-mediated therapy against multiple cell lines. Using breast cancer cell lines that represent varying levels of drug resistance to optimize drug efficacy and control cell lines to optimize treatment safety, the FSC.II platform was able to reconcile experimental phenotypic response to home in on the global therapeutic window maximum. Furthermore, FSC.II was able to optimize ND–drug combinations to outperform ND–single drug and unmodified single-drug therapy as well as optimal unmodified drug therapy. In addition, FSC.II was able to pinpoint a ND–drug combination that outperformed randomly sampled ND–drug combinations. This work confirmed that FSC.II is not a predictive but rather a convergent and deterministic platform that will enable the rational and systematic design of drug combinations for individual or population-optimized medicine.

## MATERIALS AND METHODS

**Synthesis and Characterization of Nanodiamond-Modified Drugs.** Nanodiamonds were obtained from the NanoCarbon Research Institute Ltd. (Nagano, Japan). Doxorubicin hydrochloride and mitoxantrone dihydrochloride were purchased from Sigma-Aldrich (Milwaukee, WI, USA), and bleomycin sulfate was acquired from Cayman Chemical (Ann Arbor, MI, USA). All samples and solvents were autoclaved prior to use. To formulate the ND–drug complexes, the drugs were mixed with sterilized deionized water at 5 mg/mL. Autoclaved NDs were then mixed at a ratio of 5:1 (w/w) with doxorubicin and mitoxantrone and 5:2 (w/w) with bleomycin, followed by the addition of NaOH for coupling drugs onto the NDs to a final NaOH concentration of 2.5 mM. The ND–drugs were mixed thoroughly and incubated for 4 days at room temperature. Subsequently, the ND–drug suspensions were centrifuged and washed with deionized water until transparent ND–drug solutions were obtained. The final products were resuspended in water with concentrations of 5 mg/mL (ND/water, w/v) for loading efficiency and nanoparticle characterization.

During the washing/centrifuging steps, supernatants containing unbound drugs were analyzed to determine the drug loading efficiencies. We measured the absorbance of the supernatant containing free DOX, MTX, and BLEO at 550, 590, and 290 nm, respectively. We calculated the concentration of drug incorporated onto the NDs *via* standard curves which were set by the absorbance values of serial dilutions of the drugs with a range from 0 to 200  $\mu$ g/mL.

To confirm drug presence on the NDs, FTIR spectroscopy was performed (Jasco FT/IR-420). Prior to FTIR analysis, 2 mg of ND, drugs, and ND–drug samples were mixed with 100 mg of potassium bromide by using mortar and pestle and then pelletized to make thin discs for further analyses with the resolution of 1  $\text{cm}^{-1}$  and 64 scan accumulations.

The size and  $\zeta$ -potential of NDs and ND–drug complexes (0.2–0.3 mg/mL) were measured using a Zetasizer Nano ZS (Malvern Instrument, UK). Nanoparticle sizes were measured at a 173° backscattering angle with at least three runs at 25 °C. The hydrodynamic diameter was determined from the z-average values from runs in triplicate. The  $\zeta$ -potential was also determined at 25 °C in water by using DTS-1060C clear zeta cells in automatic mode.

**Cell Culture and Plating.** MCF10A (human epithelial breast cells), H9C2 (rat myocardium myoblast cells), IMR-90 (human lung fibroblast cells), BT20 (human breast carcinoma cells),

MCF7 (human breast carcinoma cells), and MDA-MB-231 (human breast adenocarcinoma cells) were obtained from American Type Culture Collection (ATCC) and were cultured according to manufacturer protocols. Cells were subsequently detached *via* trypsin-EDTA, counted *via* a hemocytometer (Hausser), and seeded into 96-well plates *via* a Biomek FXp (Beckman Coulter).

**Single Drug and Drug Combination Evaluation.** For the single-drug study, unmodified and ND-modified doxorubicin, bleomycin, and mitoxantrone were used. Paclitaxel was used in the unmodified version. Serial dilutions of the drugs were made on a 96-well plate and then applied to the corresponding wells on a cell plate. These steps were repeated for the remaining cell lines. For the drug combination study, concentrations of drugs were determined using the outcome of the single-drug experiments. ND drugs or unmodified drugs were applied onto a 48-well plate, and serial dilutions were made. Drug combinations, according to Latin hypercube sampling, were then made on a 96-well plate. These drug solutions were then transferred to the corresponding wells on a cell plate. These procedures were applied for all cell plates. Cells were incubated in drug solutions at 37 °C for 72 h.

**Cell Viability Assays.** To determine cell viability, 0.5 mM resazurin (Sigma) was applied to the 96-well cell plates, followed by an incubation period of 3 h at 37 °C and 5% CO<sub>2</sub>. Cell viability was measured by fluorescence readings at 560 nm/590 nm.

**Latin Hypercube Sampling.** The drug concentration range was determined by single-drug dose–response experiments of the cancer model to be between the maximum achievable concentration and the zero effect concentration. We then took the log concentration and discretized the log concentration range of each drug into seven strata. A Latin hypercube sampling process was performed on the sample space, ensuring that all subspaces were comprehensively covered. Following objective function determination in order to account for maximal therapeutic efficacy against the cancer cell lines while minimizing toxicity against control cell lines, differential evolution was applied to rapidly identify globally optimized drug combinations for subsequent verification.

Latin hypercube sampling was performed upon the sample space  $\Omega$ , where the input  $X \in \Omega^N$ . Let the sample be  $X_{ij}$ ,  $i = 1, \dots, N$  and  $j = 1, \dots, K$ . We discretize the range of  $X_i$  into  $N$  strata, and a component from each stratum was selected. The components were rounded up to the closest digits and treated as stages in

the log concentration range. Each sampled component was randomly assigned into the final design matrix  $X$ . In this way,  $\Omega$  was divided into  $N^k$  cells, which represented a hypercube discretization of the sample space. The Latin hypercube sampling process ensured that all subspaces of  $\Omega$  were fully covered, and the components were sampled in a stratified manner.

**Statistical Analysis.** A student *t* test was utilized for statistical analysis of FSC-based optimization of nanodiamond–drug combinations. Analysis was completed for studies comparing FSC-optimized nanodiamond-modified combinations with modified and unmodified single drugs, unmodified drug combinations, as well as randomly sampled nanodiamond-modified combinations. A *p* value of less than 0.05 was deemed to represent statistical significance in these cases. For the response surface formulation studies, a *t* test with the hypothesis that the experimental window was derived from normal distribution with the mean as the prediction and unknown variance was conducted. Therefore, the null hypothesis was considered to pass if the prediction and experimental values matched. Pearson correlation analysis was also plotted to further correlate FSC prescriptions with experimental verification.

**Conflict of Interest:** The authors declare the following competing financial interest(s): H.W., D.-K.L., K.-Y.C., K.Z., A.S., C.-M.H., and D.H. are inventors on filed patents pertaining to FSC.II.

**Acknowledgment.** D.H. gratefully acknowledges support from the National Science Foundation CAREER Award (CMMI-1350197), Center for Scalable and Integrated NanoManufacturing (DMI-0327077), CMMI-0856492, DMR-1343991, V Foundation for Cancer Research Scholars Award, Wallace H. Coulter Foundation Translational Research Award, National Cancer Institute Grant U54CA151880 (the content is solely the responsibility of the authors and does not necessarily represent the official views of the National Cancer Institute or the National Institutes of Health), Society for Laboratory Automation and Screening Endowed Fellowship, and Beckman Coulter Life Sciences.

**Supporting Information Available:** Drug loading characterization; nanoparticle combination versus unmodified single-drug therapy analysis; dilution information; Latin hypercube sampling information. This material is available free of charge via the Internet at <http://pubs.acs.org>.

## REFERENCES AND NOTES

- Zhao, B.; Pritchard, J. R.; Lauffenburger, D. A.; Hemann, M. T. Addressing Genetic Tumor Heterogeneity through Computationally Predictive Combination Therapy. *Cancer Discovery* **2014**, *4*, 166–174.
- Al-Lazikani, B.; Banerji, U.; Workman, P. Combinatorial Drug Therapy for Cancer in the Post-genomic Era. *Nat. Biotechnol.* **2012**, *30*, 679–692.
- Kummar, S.; Chen, H. X.; Wright, J.; Holbeck, S.; Millin, M. D.; Tomaszewski, J.; Zweibel, J.; Collins, J.; Doroshow, J. H. Utilizing Targeted Cancer Therapeutic Agents in Combination: Novel Approaches and Urgent Requirements. *Nat. Rev. Drug Discovery* **2010**, *9*, 843–856.
- Munos, B. Lessons from 60 Years of Pharmaceutical Innovation. *Nat. Rev. Drug Discovery* **2009**, *8*, 959–968.
- Fitzgerald, J. B.; Schoeberl, B.; Nielsen, U. B.; Sorger, P. K. Systems Biology and Combination Therapy in the Quest for Clinical Efficacy. *Nat. Chem. Biol.* **2006**, *2*, 458–466.
- Kreeger, P. K.; Lauffenburger, D. A. Cancer Systems Biology: A Network Modeling Perspective. *Carcinogenesis* **2010**, *31*, 2–8.
- Barabasi, A.-L.; Oltvai, Z. N. Network Biology: Understanding the Cell's Functional Organization. *Nat. Rev. Genet.* **2004**, *5*, 101–113.
- Watts, D. J.; Strogatz, S. H. Collective Dynamics of 'Small-World' Networks. *Nature* **1998**, *393*, 440–442.
- Jeong, H.; Tombor, B.; Albert, R.; Oltvai, Z. N.; Barabasi, A.-L. The Large Scale Organization of Metabolic Networks. *Nature* **2000**, *407*, 651–654.
- Hood, L.; Heath, J. R.; Phelps, M. E.; Lin, B. Systems Biology and New Technologies Enable Predictive and Preventative Medicine. *Science* **2004**, *306*, 640–643.
- Persidis, A. Cancer Multidrug Resistance. *Nat. Biotechnol.* **1999**, *17*, 94–95.
- Gottesman, M. M.; Fojo, T.; Bates, S. E. Multidrug Resistance in Cancer: Role of ATP-Dependent Transporters. *Nat. Rev. Cancer* **2002**, *2*, 48–58.
- Doyle, L. A.; Yang, W.; Abruzzo, L. V.; Krogmann, T.; Gao, Y.; Rishi, A. K.; Ross, D. D. A Multidrug Resistance Transporter from Human MCF-7 Breast Cancer Cells. *Proc. Natl. Acad. Sci. U.S.A.* **1998**, *95*, 15665–15670.
- Goldstein, L. J.; Galski, H.; Fojo, A.; Willingham, M.; Lai, S.-L.; Gazdar, A.; Pirker, R.; Green, A.; Crist, W.; Brodeur, G. M.; et al. Expression of Multidrug Resistance Gene in Human Cancers. *J. Natl. Cancer Inst.* **1989**, *81*, 116–124.
- Lage, H. An Overview of Cancer Multidrug Resistance: A Still Unsolved Problem. *Cell. Mol. Life Sci.* **2008**, *65*, 3145–3167.
- Cole, S. P.; Bhardwaj, G.; Gerlach, J. H.; Mackie, J. E.; Grant, C. E.; Almquist, K. C.; Stewart, A. J.; Kurz, E. U.; Duncan, A. M.; Deeley, R. G. Overexpression of a Transporter Gene in a Multidrug-Resistant Human Lung Cancer Cell Line. *Science* **1992**, *258*, 1650–1654.
- Ágoston, V.; Csermely, P.; Pongor, S. Multiple Weak Hits Confuse Complex Systems: A Transcriptional Regulatory Network as an Example. *Phys. Rev. E* **2005**, *71*, 051909.
- Bozic, I.; Reiter, J. G.; Allen, B.; Antal, T.; Chatterjee, K.; Shah, P.; Moon, Y. S.; Yaqubie, A.; Kelly, N.; Le, D. T.; et al. Evolutionary Dynamics of Cancer in Response to Targeted Combination Therapy. *eLife* **2013**, *2*, e00747.
- Holmes, F. A.; Walters, R. S.; Theriault, R. L.; Buzdar, A. U.; Frye, D. K.; Hortobagyi, G. N.; Forman, A. D.; Newton, L. K.; Raber, M. N. Phase II Trial of Taxol, an Active Drug in the Treatment of Metastatic Breast Cancer. *J. Natl. Cancer Inst.* **1991**, *83*, 1797–1805.
- Hellman, S.; Rosenberg, S. A.; DeVita, V. T. *Cancer: Principles & Practice of Oncology*; Lippincott-Raven: Philadelphia, PA, 1997; Vol. 2.
- Ciardiello, F.; Caputo, R.; Bianco, R.; Damiano, V.; Pomato, G.; De Placido, S.; Bianco, A. R.; Tortora, G. Antitumor Effect and Potentiation of Cytotoxic Drugs Activity in Human Cancer Cells by ZD-1839 (Iressa), an Epidermal Growth Factor Receptor-Selective Tyrosine Kinase Inhibitor. *Clin. Cancer Res.* **2000**, *6*, 2053–2063.
- de Gramont, A. D.; Figer, A.; Seymour, M.; Homerin, M.; Hmissi, A.; Cassidy, J.; Boni, C.; Cortes-Funes, H.; Cervantes, A.; Freyer, G.; et al. Leucovorin and Fluorouracil with or without Oxaliplatin as First-Line Treatment in Advanced Colorectal Cancer. *J. Clin. Oncol.* **2000**, *18*, 2938–2947.
- O'Shaughnessy, J.; Miles, D.; Vukelja, S.; Moiseyenko, V.; Ayoub, J.-P.; Cervantes, G.; Fumoleau, P.; Jones, S.; Lui, W.-Y.; Mauriac, L.; et al. Superior Survival with Capecitabine Plus Docetaxel Combination Therapy in Anthracycline-Pretreated Patients with Advanced Breast Cancer: Phase III Trial Results. *J. Clin. Oncol.* **2002**, *20*, 2812–2823.
- Goldberg, R. M.; Sargent, D. J.; Morton, R. F.; Fuchs, C. S.; Ramanathan, R. K.; Williamson, S. K.; Findlay, B. P.; Pitot, H. C.; Alberts, S. R. A Randomized Controlled Trial of Fluorouracil Plus Leucovorin, Irinotecan, and Oxaliplatin Combinations in Patients with Previously Untreated Metastatic Colorectal Cancer. *J. Clin. Oncol.* **2004**, *22*, 23–30.
- Peppas, N. A.; Hilt, J. Z.; Khademhosseini, A.; Langer, R. Hydrogels in Biology and Medicine: From Molecular Principles to Bionanotechnology. *Adv. Mater.* **2006**, *18*, 1345–1360.
- Colombo, M.; Carregal-Romero, S.; Casula, M. F.; Gutiérrez, L.; Morales, M. P.; Böhm, I. B.; Heverhagen, J. T.; Prosperi, D.; Parak, W. J. Biological Applications of Magnetic Nanoparticles. *Chem. Soc. Rev.* **2012**, *41*, 4306–4334.
- Montenegro, J.-M.; Grazu, V.; Sukhanova, A.; Agarwal, S.; de la Fuente, J. M.; Nabiev, I.; Greiner, A.; Parak, W. J. Controlled Antibody/(Bio-) Conjugation of Inorganic Nanoparticles for Targeted Delivery. *Adv. Drug Delivery Rev.* **2013**, *65*, 677–688.
- Farokhzad, O. C.; Jon, S.; Khademhosseini, A.; Tran, T.-N. T.; LaVan, D. A.; Langer, R. Nanoparticle–Aptamer

- Bioconjugates a New Approach for Targeting Prostate Cancer Cells. *Cancer Res.* **2004**, *64*, 7668–7672.
29. Xu, X.; Xie, K.; Zhang, X.-Q.; Pridgen, E. M.; Park, G. Y.; Cui, D. S.; Shi, J.; Wu, J.; Kantoff, P. W.; Lippard, S. J.; et al. Enhancing Tumor Cell Response to Chemotherapy through Nanoparticle-Mediated Codelivery of siRNA and Cisplatin Prodrug. *Proc. Natl. Acad. Sci. U.S.A.* **2013**, *110*, 18638–18643.
  30. Zhang, X.-Q.; Xu, X.; Lam, R.; Giljohann, D.; Ho, D.; Mirkin, C. A. Strategy for Increasing Drug Solubility and Efficacy through Covalent Attachment to Polyvalent DNA–Nanoparticle Conjugates. *ACS Nano* **2011**, *5*, 6962–6970.
  31. Dhar, S.; Daniel, W. L.; Giljohann, D. A.; Mirkin, C. A.; Lippard, S. J. Polyvalent Oligonucleotide Gold Nanoparticle Conjugates as Delivery Vehicles for Platinum (IV) Warheads. *J. Am. Chem. Soc.* **2009**, *131*, 14652–14653.
  32. Gharpure, K. M.; Chu, K. S.; Bowerman, C.; Miyake, T.; Pradeep, S.; Mangala, L. S.; Han, H.-D.; Rupaimoole, R.; Armaiz-Pena, G. N.; Rahhal, T. B.; et al. Metronomic Docetaxel in PRINT® Nanoparticles and EZH2 Silencing Have Synergistic Antitumor Effect in Ovarian Cancer. *Mol. Cancer Ther.* **2014**, *13*, 1750–1757.
  33. Von Maltzahn, G.; Park, J.-H.; Lin, K. Y.; Singh, N.; Schwöppe, C.; Mesters, R.; Berdel, W. E.; Ruoslahti, E.; Sailor, M. J.; Bhatia, S. N. Nanoparticles That Communicate *In Vivo* To Amplify Tumour Targeting. *Nat. Mater.* **2011**, *10*, 545–552.
  34. Uskokovic, V.; Lee, K.; Lee, P. P.; Fischer, K. E.; Desai, T. A. Shape Effect in the Design of Nanowire-Coated Microparticles as Transepithelial Drug Delivery Devices. *ACS Nano* **2012**, *6*, 7832–7841.
  35. Chirra, H. D.; Desai, T. A. Multi-reservoir Bioadhesive Micro-devices for Independent Rate-Controlled Delivery of Multiple Drugs. *Small* **2012**, *8*, 3839–3846.
  36. Davis, M. E.; Zuckerman, J. E.; Choi, C. H. J.; Seligson, D.; Tolcher, A.; Alabi, C. A.; Yen, Y.; Heidel, J. D.; Ribas, A. Evidence of RNAi in Humans from Systemically Administered siRNA via Targeted Nanoparticles. *Nature* **2010**, *464*, 1067–1070.
  37. Creixell, M.; Peppas, N. A. Co-delivery of siRNA and Therapeutic Agents Using Nanocarriers To Overcome Cancer Resistance. *Nano Today* **2012**, *7*, 367–379.
  38. Perrault, S. D.; Chan, W. C. *In Vivo* Assembly of Nanoparticle Components To Improve Targeted Cancer Imaging. *Proc. Natl. Acad. Sci. U.S.A.* **2010**, *107*, 11194–11199.
  39. Eltoukhy, A. A.; Chen, D.; Alabi, C. A.; Langer, R.; Anderson, D. G. Degradable Terpolymers with Alkyl Side Chains Demonstrate Enhanced Gene Delivery Potency and Nanoparticle Stability. *Adv. Mater.* **2013**, *25*, 1487–1493.
  40. Gobin, A. M.; Lee, M. H.; Halas, N. J.; James, W. D.; Drezek, R. A.; West, J. L. Near-Infrared Resonant Nanoshells for Combined Optical Imaging and Photothermal Cancer Therapy. *Nano Lett.* **2007**, *7*, 1929–1934.
  41. Chow, E. K.; Zhang, X.-Q.; Chen, M.; Lam, R.; Robinson, E.; Huang, H.; Schaffer, D.; Osawa, E.; Goga, A.; Ho, D. Nanodiamond Therapeutic Delivery Agents Mediate Enhanced Chemoresistant Tumor Treatment. *Sci. Transl. Med.* **2011**, *3*, 73ra21.
  42. Chow, E. K.-H.; Ho, D. Cancer Nanomedicine: From Drug Delivery to Imaging. *Sci. Transl. Med.* **2013**, *5*, 216rv4.
  43. Moore, L.; Chow, E. K. H.; Osawa, E.; Bishop, J. M.; Ho, D. Diamond–Lipid Hybrids Enhance Chemotherapeutic Tolerance and Mediate Tumor Regression. *Adv. Mater.* **2013**, *25*, 3532–3541.
  44. Chen, M.; Pierstorff, E. D.; Lam, R.; Li, S.-Y.; Huang, H.; Osawa, E.; Ho, D. Nanodiamond-Mediated Delivery of Water-Insoluble Therapeutics. *ACS Nano* **2009**, *3*, 2016–2022.
  45. Toh, T. B.; Lee, D.-K.; Hou, W.; Abdullah, L. N.; Nguyen, J.; Ho, D.; Chow, E. Nanodiamond–Mitoxantrone Complexes Enhance Drug Retention in Chemoresistant Breast Cancer Cells. *Mol. Pharmaceutics* **2014**, *11*, 2683–2691.
  46. Loewe, S. The Problem of Synergism and Antagonism of Combined Drugs. *Arzneimittelforschung* **1953**, *3*, 285–290.
  47. Chou, T.-C.; Talalay, P. Quantitative Analysis of Dose-Effect Relationships: The Combined Effects of Multiple Drugs or Enzyme Inhibitors. *Adv. Enzyme Regul.* **1984**, *22*, 27–55.
  48. Bliss, C. The Calculation of Microbial Assays. *Bacteriol. Rev.* **1956**, *20*, 243–258.
  49. Wong, P. K.; Yu, F.; Shahangian, A.; Cheng, G.; Sun, R.; Ho, C.-M. Closed-Loop Control of Cellular Functions Using Combinatory Drugs Guided by a Stochastic Search Algorithm. *Proc. Natl. Acad. Sci. U.S.A.* **2008**, *105*, 5105–5110.
  50. Valamehr, B.; Tsutsui, H.; Ho, C.-M.; Wu, H. Developing Defined Culture Systems for Human Pluripotent Stem Cells. *Regener. Med.* **2011**, *6*, 623–634.
  51. Al-Shyoukh, I.; Yu, F.; Feng, J.; Yan, K.; Dubinett, S.; Ho, C.-M.; Shamma, J. S.; Sun, R. Systematic Quantitative Characterization of Cellular Responses Induced by Multiple Signals. *BMC Syst. Biol.* **2011**, *5*, 88.
  52. Yu, F.; Al-Shyoukh, I.; Feng, J.; Li, X.; Liao, C. W.; Ho, C.-M.; Shamma, J. S.; Sun, R. Control of Kaposi's Sarcoma-Associated Herpesvirus Reactivation Induced by Multiple Signals. *PLoS One* **2011**, *6*, e20998.
  53. Wei, F.; Bai, B.; Ho, C.-M. Rapidly Optimizing an Aptamer Based BoNT Sensor by Feedback System Control (FSC) Scheme. *Biosens. Bioelectron.* **2011**, *30*, 174–179.
  54. Yu, H.; Zhang, W. L.; Ding, X.; Zheng, K. Y.; Ho, C.-M.; Tsim, K. W.; Lee, Y.-K. Optimizing Combinations of Flavonoids Deriving from Astragalus Radix in Activating the Regulatory Element of Erythropoietin by a Feedback System Control Scheme. *J. Evidence-Based Complementary Altern. Med.* **2013**, *541436*.
  55. Ding, X.; Sanchez, D. J.; Shahangian, A.; Al-Shyoukh, I.; Cheng, G.; Ho, C.-M. Cascade Search for HSV-1 Combinatorial Drugs with High Antiviral Efficacy and Low Toxicity. *Int. J. Nanomed.* **2012**, *7*, 2281–2292.
  56. Wang, H.; Silva, A.; Ho, C.-M. When Medicine Meets Engineering—Paradigm Shifts in Diagnostics and Therapeutics. *Diagnostics* **2013**, *3*, 126–154.
  57. Honda, Y.; Ding, X.; Mussano, F.; Wiberg, A.; Ho, C.-M.; Nishimura, I. Guiding the Osteogenic Fate of Mouse and Human Mesenchymal Stem Cells through Feedback System Control. *Sci. Rep.* **2013**, *3*, 3420.
  58. Tsutsui, H.; Valamehr, B.; Hindoyan, A.; Qiao, R.; Ding, X.; Guo, S.; Witte, O. N.; Liu, X.; Ho, C.-M.; Wu, H. An Optimized Small Molecule Inhibitor Cocktail Supports Long-Term Maintenance of Human Embryonic Stem Cells. *Nat. Commun.* **2011**, *2*, 167.
  59. Ding, X.; Xu, H.; Hopper, C.; Yang, J.; Ho, C. M. Use of Fractional Factorial Designs in Antiviral Drug Studies. *Qual. Reliab. Eng. Int.* **2013**, *29*, 299–304.
  60. McKay, M. D.; Beckman, R. J.; Conover, W. J. Comparison of Three Methods for Selecting Values of Input Variables in the Analysis of Output from a Computer Code. *Technometrics* **1979**, *21*, 239–245.
  61. Storn, R.; Price, K. Differential Evolution—A Simple and Efficient Heuristic for Global Optimization over Continuous Spaces. *J. Global Optim.* **1997**, *11*, 341–359.
  62. Liang, Y.; Ozawa, M.; Krueger, A. A General Procedure To Functionalize Agglomerating Nanoparticles Demonstrated on Nanodiamond. *ACS Nano* **2009**, *3*, 2288–2296.
  63. Barnard, A. S. Diamond Standard in Diagnostics: Nanodiamond Biolabels Make Their Mark. *Analyst* **2009**, *134*, 1751–1764.
  64. Barnard, A. S. Self-Assembly in Nanodiamond Agglutinates. *J. Mater. Chem.* **2008**, *18*, 4038–4041.
  65. McGuinness, L. P.; Yan, Y.; Stacey, A.; Simpson, D. A.; Hall, L. T.; Maclaurin, D.; Prawer, S.; Mulvaney, P.; Wrachtrup, J.; Caruso, F.; et al. Quantum Measurement and Orientation Tracking of Fluorescent Nanodiamonds Inside Living Cells. *Nat. Nanotechnol.* **2011**, *6*, 358–363.
  66. Mohan, N.; Chen, C.-S.; Hsieh, H.-H.; Wu, Y.-C.; Chang, H.-C. *In Vivo* Imaging and Toxicity Assessments of Fluorescent Nanodiamonds in *Caenorhabditis elegans*. *Nano Lett.* **2010**, *10*, 3692–3699.
  67. Mochalin, V. N.; Gogotsi, Y. Wet Chemistry Route to Hydrophobic Blue Fluorescent Nanodiamond. *J. Am. Chem. Soc.* **2009**, *131*, 4594–4595.
  68. Chang, L.-Y.; Osawa, E.; Barnard, A. S. Confirmation of the Electrostatic Self-Assembly of Nanodiamonds. *Nanoscale* **2011**, *3*, 958–962.

69. Barnard, A. S.; Sternberg, M. Crystallinity and Surface Electrostatics of Diamond Nanocrystals. *J. Mater. Chem.* **2007**, *17*, 4811–4819.
70. Barnard, A. S.; Osawa, E. The Impact of Structural Polydispersity on the Surface Electrostatic Potential of Nano-diamond. *Nanoscale* **2014**, *6*, 1188–1194.
71. Cohen, J. *Statistical Power Analysis for the Behavioral Sciences*; Taylor and Francis: New York, 1988.
72. Xi, G.; Robinson, E.; Mania-Farnell, B.; Vanin, E. F.; Shim, K.-W.; Takao, T.; Allender, E. V.; Mayanil, C. S.; Soares, M. B.; Ho, D.; et al. Convection-Enhanced Delivery of Nano-diamond Drug Delivery Platforms for Intracranial Tumor Treatment. *Nanomedicine* **2014**, *10*, 381–391.
73. Wood, K.; Nishida, S.; Sontag, E. D.; Cluzel, P. Mechanism-Independent Method for Predicting Response to Multi-drug Combinations in Bacteria. *Proc. Natl. Acad. Sci. U.S.A.* **2012**, *109*, 12254–12259.
74. Giordano, S.; Petrelli, A. From Single- to Multi-target Drugs in Cancer Therapy: When Aspecificity Becomes an Advantage. *Curr. Med. Chem.* **2008**, *15*, 422–432.
75. Gottesman, M. M. Mechanisms of Cancer Drug Resistance. *Annu. Rev. Med.* **2002**, *53*, 615–627.
76. Jänne, P. A.; Gray, N.; Settleman, J. Factors Underlying Sensitivity of Cancers to Small-Molecule Kinase Inhibitors. *Nat. Rev. Drug Discovery* **2009**, *8*, 709–723.
77. Komarova, N. L.; Wodarz, D. Drug Resistance in Cancer: Principles of Emergence and Prevention. *Proc. Natl. Acad. Sci. U.S.A.* **2005**, *102*, 9714–9719.
78. Hrkach, J.; Von Hoff, D.; Ali, M. M.; Andrianova, E.; Auer, J.; Campbell, T.; De Witt, D.; Figa, M.; Figueiredo, M.; Horhota, A.; et al. Precinical Development and Clinical Translation of a PSMA-Targeted Docetaxel Nanoparticle with a Differentiated Pharmacological Profile. *Sci. Transl. Med.* **2012**, *4*, 128ra39.
79. Sun, W.; Jiang, T.; Lu, Y.; Reiff, M.; Mo, R.; Gu, Z. Cocoon-like Self-Degradable DNA-Nanoclew for Anticancer Drug Delivery. *J. Am. Chem. Soc.* **2014**, *136*, 14722–14725.
80. Lu, Y.; Mo, R.; Tai, W.; Sun, W.; Pacardo, D. B.; Qian, C.; Shen, Q.; Ligler, F. S.; Gu, Z. Self-Folded Redox/Acid Dual-Responsive Nanocarriers for Anticancer Drug Delivery. *Chem. Commun.* **2014**, *50*, 15105–15108.
81. Lehmann, B. D.; Bauer, J. A.; Chen, X.; Sanders, M. E.; Chakravarthy, A. B.; Shyr, Y.; Pietenpol, J. A. Identification of Human Triple-Negative Breast Cancer Subtypes and Preclinical Models for Selection of Targeted Therapies. *J. Clin. Invest.* **2011**, *121*, 2750–2767.
82. Yamori, T. Panel of Human Cancer Cell Lines Provides Valuable Database for Drug Discovery and Bioinformatics. *Cancer Chemother. Pharmacol.* **2003**, *52*, 74–79.
83. Iorio, M. V.; Ferracin, M.; Liu, C.-G.; Veronese, A.; Spizzo, R.; Sabbioni, S.; Magri, E.; Pedriali, M.; Fabbri, M.; Campiglio, M.; et al. MicroRNA Gene Expression Deregulation in Human Breast Cancer. *Cancer Res.* **2005**, *65*, 7065–7070.